

Capacitive touchscreen sensing - a measure of electrolyte conductivity

Sebastian Horstmann^{a,b,*}, Cassi J Henderson^a, Elizabeth A H Hall^{b*}, Ronan Daly^{a*}

^a *Department of Engineering, University of Cambridge, Charles Babbage Road, Cambridge, CB3 0FS.*

^b *Department of Chemical Engineering and Biotechnology, University of Cambridge, Philippa Fawcett Drive, Cambridge, CB3 0AS.*

* Corresponding author. *Email address:* eah16@cam.ac.uk (E.A.H. Hall), rd439@cam.ac.uk (R. Daly), sh969@cam.ac.uk (S. Horstmann)

Abstract

Mobile technologies such as smartphones and tablets combine computational power with inbuilt sensors and networking capabilities, making them ideal measurement instruments. There is already a rich history of research and commercially manufactured accessories taking advantage of their sensing and data visualisation capabilities. However, to-date the touchscreen component has not yet been translated to the widely established fields of capacitance-based bio- and environmental sensing. Here, we demonstrate the concept of contactless conductivity sensing of fluid samples placed directly on top of a projected mutual capacitive touchscreen with the measurement of a variety of electrolytes, leveraging the touchscreen's multi-touch capabilities. Electrolyte ions are particularly susceptible to the electric fringe field induced by capacitive touchscreens, and we report here a near-linear response to the ionic concentration of metal cations interesting for drinking water quality and soil health monitoring across a range of 0 to 500 μM (up to 100 μS). Simulation results are compared with experimental findings to reveal both the working principles and the key parameters that will be important for future sensing applications. This sensor demonstration is a starting point for broader exploration of the use of projected touchscreen sensing in mobile technologies and the creation of tools that are accessible to everyone, allowing rapid measurements and communication of data.

Keywords: Electrolyte, Touchscreen, Capacitive sensing, COMSOL, Water quality, Soil health

1 Introduction

Since smartphones became widespread in the mid-2000s, there have been attempts to leverage their computational power and networking capabilities for environmental monitoring and health sensing purposes [1]. Most approaches have relied on cable- or Bluetooth-linked accessories, such as lab-on-a-chip add-ons or handheld devices, transferring their measurement results for visualisation, interpretation and storage. Only a few techniques exploit the embedded sensors in smartphones and the vast majority focus on using the camera sensor for imaging [2, 3].

Projected capacitive touchscreens are the prevalent technology for user interaction in almost every mobile device today [4] because of their precision, multi-touch capabilities and high light transmittance for integration with quality display technologies [5]. Capacitive touch sensing has already grown beyond phones towards tablets and smartwatches and is anticipated to remain a driver of future wearable technology in the coming years [6, 7]. Despite the touch sensor's prevalence, there are very few examples of using this component for fluid sensing. One notable example from Won et al. explored the potential of using the surface capacitive touchscreen technology as a DNA detection platform [8, 9, 10]. In this case, the sensor needed to be specially fabricated by patterning ITO on a glass wafer because the sample needed to be deposited directly on a functionalised electrode under laboratory conditions to measure a response. However, direct electrode contact methods need custom hardware that is not possible with smartphone or tablet devices, where the touch sensors are protected by a transparent layer of glass. Here, we explore the core capability of the measurement of ionic compounds within aqueous fluids, namely electrolytes, which have been deposited on an industry-standard mutual capacitive touchscreen to take a step towards the vision of direct-to-screen sensing. As ions interact with the electric fields generated by touchscreens, we use the fringe field interactions to register properties of electrolyte solutions, as illustrated in Figure 1 (a). Drops sit on the electrode array, separated from making direct electrode contact by a thin insulating layer, as shown in Figures 1(b), (c).

Electrolytes are a natural and nutritional component of drinking water and cultivated soil everywhere in the world; however, the growing pollution of surface waters introduces unhealthy ions and limits access to clean water for over a quarter of the world's population [11]. Most ions in drinking water are not harmful to human health, but the contamination of some metal ions, such as arsenic and lead, are carcinogenic or can lead to organ dysfunction and others, such as nitrate and phosphate, can harm natural ecosystems when processed water leaks into the environment [12]. The lack of ions such as nitrogen, phosphorus, and potassium (NPK) fertilising agricultural soil can impair crop yields necessary for feeding a growing human population [13]. There are usually only trace levels of these ions (ppb or μM range) and samples require transport to a laboratory and analysis with benchtop equipment far away from the source of extraction [14, 15]. Extending the capabilities of smartphones towards electrolyte sensing in water and soil samples would help people to make an informed decision before exposing themselves to the risk of drinking contaminated water and could help in the prevention of many health threats as well as early child death in regions struggling with malnutrition and drinking water pollution.

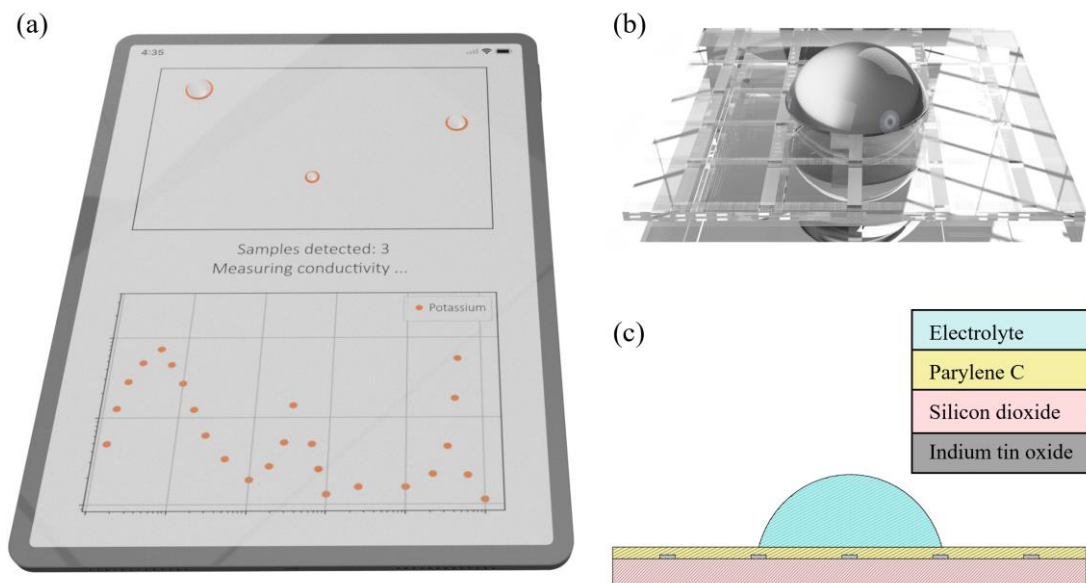


Figure 1: (a) Future concept of a tablet-based touchscreen electrolyte sensor. (b) A rendering of a sample drop deposited on a silicon dioxide (glass) and indium tin oxide (ITO)-based transparent capacitive touch sensor. (c) The sensor cross-section showing a parylene C layer fabricated between the electrodes and the sample electrolyte.

As a first step, we demonstrate the feasibility of measuring the electrolyte concentration of a fluid from a touchscreen sensor, using the standard test capabilities and equipment when manufacturing touchscreen mobile technologies. We then detail the key parameters that need to be controlled to enhance the reproducibility of such measurements. The multi-touch capability of a touchscreen in mutual capacitive mode is examined as a route to measuring multiple sample-drops at once, to allow error reduction when required, measurement of a reference, and, in the future, multiplexed sensing. A simulation of the full system in COMSOL Multiphysics is also demonstrated for comparison with experimental results and to test the feasibility of using the simulation as a predictive tool for guiding designs. Through using an industrially-provided touchscreen technology and testing equipment, this approach for electrolyte conductivity measurements is expected to be compatible with existing hardware in smartphones and tablets and is envisioned to be a key step towards environmental measurements that can be seamlessly performed, analysed and communicated using a single device.

2 Methods

2.1 Materials and chemicals

All measurements have been conducted using a commercially available TouchNetix capacitive touchscreen device (TNxS00119) by MSolv Ltd. The manufacturers provided this as a non-device-integrated test board, allowing flexibility and access to measurement acquisition as described below in Section 2.2. The device consists of a 0.7 mm thick sheet of silicon dioxide glass coated with a 25 nm layer of indium tin oxide on both sides. As indicated in Figure 2, there is a horizontal (bottom side) and a vertical (top side) electrode array with an average pitch of 1.7mm. For comparison we note, other device-integrated commercial touchscreens studied in previous literature have a considerably larger pitch size of 3.5mm (LG smartwatch), 3.9mm (Samsung S4 phone), 4.0mm (Samsung S2 Tablet), 4.1mm (Nexus 5 smartphone), and ~5.9mm (Microsoft Surface 55") [16]. As the ITO structure of most modern mobile-integrated capacitive touchscreens is protected by a sheet of glass ($\epsilon_{r, \text{glass}} \approx 4.2$), we decided to coat the surface using a polymer ($\epsilon_{r, \text{parlylene}} \approx 2.7$), which is noted later to have only minimal effect on the results and can be applied with fine control of the thickness. The effect of the different permittivity of these materials on the touchscreen readout is discussed using a simulation in Section 3.1. We prepared the touchscreen device with parlylene C (poly(p-xylylene) polymer) using a vapour deposition process [17], for which an SCS PDS 2010 Labcoater 2 has been used (see details in Supplementary Information S1). Sodium chloride, sodium acetate, calcium chloride, iron (III) chloride hexahydrate, magnesium chloride (all $\geq 99\%$ anhydrous, Merck / Sigma Aldrich), and potassium chloride (99%, Fisher Scientific) were used as received. Stock solutions of the respective metal chlorides were prepared by gently adding 10 mmol salt to 100 mL Milli-Q water followed by vigorous stirring. The volume was adjusted to 1000 mL with Milli-Q water to achieve a bulk concentration of 10 mM. The bulk solutions have been further diluted using de-ionised (DI) water (Sigma-Aldrich) in advance of a measurement on the same day.

2.2 Measurement principle

Each top and bottom electrode is controlled by an electric controller printed circuit board connected via USB which is operated using TouchNetix' readout software in Microsoft Windows. The controller includes a digital multiplexer connected to each of the 40 electrodes on the touchscreen bottom and 70 electrodes on the touchscreen top. Reading the whole touchscreen panel in the software returns an array of 70x40 mutual capacitance values C_i , which each correspond to an electrode intersection. The resulting matrix can be visualised as an image where the shade of each pixel corresponds to the capacitance measured in the corresponding electrode intersection.

An automatic detection of drops on the device is performed in post-processing using a script we developed using blob detection methods from Python computer vision libraries. One sample drop of 200 μL covers an array of multiple electrode intersections of which the centre pixel is detected. If multiple sample drops are recorded within one measurement frame, the script returns the mean and standard deviation (1 value per drop).

Before every measurement of an electrolyte concentration the baseline for each individual intersection, $C_{i,\text{ref}}$, is recorded for the dry screen. When a sample drop is deposited on the screen this baseline is subtracted automatically for every entry of the resulting $C_{i,\text{drop}}$ matrix such as indicated in Equation 1. Using this process, matrix entries C_i of intersections where no sample is detected are at 0 capacitance change, while those where a DI water drop is present are in the order of -3,000 fF.

$$C_i = C_{i,\text{drop}} - C_{i,\text{ref}} \quad (1)$$

2.3 Experimental methodology

Prior to measurements, the touchscreen is carefully cleaned by applying DI water to remove potential contamination such as dust or ionic residuals before it is dried with absorbent tissue (Kimtech). Multiple drops are deposited (number n between 6 and 24) of the same sample with 200 μL volume each (unless otherwise noted) to the parylene C coated side. Consecutive measurements are performed within a few minutes from low concentrations to high concentration without extra DI water washing steps in between. The conductivity of each measured solution is assessed immediately after each touchscreen measurement using a 5-point-calibrated Hanna Instruments HI-98192 conductivity meter. After every sequence of electrolyte measurement, a DI water cleaning step is performed before a reference DI water measurement is recorded to rule out signal drifts over the course of the experiment that might be caused by changing environmental conditions. A compilation of measurements using the same sample on different days is included in Supplementary Information S2.

2.4 Simulations

In addition to the experimental assessment, the touchscreen device has been modelled with the finite element analysis software COMSOL Multiphysics. The sample shape is approximated with a sphere section that matches the mean experimentally observed drop spread of 5.6 mm radius on the sensor surface and 3.6 mm height, equating to the deposited 200 μL liquid volume. The mathematical model for this approximation is detailed in the Supplementary Information S3.

COMSOL auto-splits the 3D model into finite elements using the physics controlled free tetrahedral mesh. A detailed mesh analysis can be found in Supplementary Information S4 and S5. To simulate mutual capacitive sensing in COMSOL a 1V terminal is assigned to the respective top electrode at a time while one bottom electrode is set to the ground level corresponding to the intersection of interest. All electrode intersections are simulated sequentially to generate the mutual capacitance value for each element on the sensor panel. All further input parameters for the COMSOL simulation are linked in Table A1 of Supplementary Information.

In addition to the mutual capacitance value, which is a global property of the system, this article also shows a measure of the local magnitude of electric field interactions on the sample: the electric displacement field. COMSOL derives the electric displacement field spatially using Equation 2 by evaluation of the local electric potential gradient and the local permittivity of the material and the absolute vacuum permittivity constant ϵ_0 . The polarisation density scales with the relative permittivity of the material and the electric field \mathbf{E} . In the case of a water drop sample on a touchscreen, the displacement field, \mathbf{D} , is dominated by the polarisation density component, \mathbf{P} , which is material dependant, scaling with its 80-times higher relative permittivity ϵ_r compared to air. Thus, the displacement field is susceptible to change in sample properties and position of the drop with respect to the electrodes.

$$\mathbf{D} = \epsilon_0 \mathbf{E} + \mathbf{P} = -\epsilon_0 \epsilon_r \nabla U \quad (2)$$

The displacement field is linked to the total free charge Q_{free} via an integral across the capacitor surface element dA following Gauss law (Equation 3).

$$\oint_A^0 \mathbf{D} \cdot d\mathbf{A} = Q_{\text{free}} \quad (3)$$

The free charge Q is, as shown in Equation 4, proportional to the mutual capacitance via the voltage U applied to the capacitor terminal.

$$C = \frac{Q_{\text{free}}}{U} \quad (4)$$

Simulated capacitance readings for this article are extracted from the Maxwell capacitance matrix $C_{1,1}$ which COMSOL outputs.

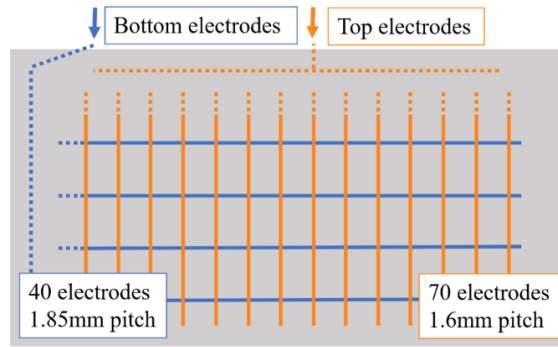


Figure 2: Simplified schematic of the top and bottom electrode structure forming the capacitor intersections. The electrodes are spaced 10% closer together on the top (1.6 mm pitch) compared to the bottom side (1.85 mm).

3 Results and Discussion

To test the feasibility of using touchscreen devices for quantitative sensing of liquid samples deposited directly on the surface, the initial step is to select a suitable sample volume for robust signal extraction (Section 3.1). We then examine in more detail the role of a protecting, electrically insulating film covering the electrodes and its influence over sensor performance (Section 3.2). Finally, we use the touchscreen for a first demonstration of its capabilities by measuring different electrolyte types and examine the correlation with their independently obtained conductivity values (Section 3.3).

3.1 Determining an appropriate sample volume for a quantitative touchscreen measurement

The core principle we wish to test is the effect of a fluid drop's polarisation field on the absolute capacitance reading from a touchscreen. The first step is to identify a robust methodology for repeatable measurements, and specifically the volume and number of droplets to measure. Figure 3(a) shows the placement of deposited fluids on the touchscreen, with examples for 1 μL , 50 μL , and 1000 μL provided, and the corresponding graphical colour map readout from the touchscreen. As features of high dielectric permittivity interact more strongly with an external voltage gradient, a water-based drop ($\epsilon_r \approx 80$) is expected to dominate the overall signal in a system that is primarily made of air, glass and polymer (all $\epsilon_r < 5$). For a low volume drop, the potential decreases by the same amount as a high-volume drop, but over a smaller scale, locally inducing an increased voltage gradient compared with a larger sample. This effect is often described as field focusing [19].

When considering future applications, it will be beneficial to make best use of sensing area and place multiple independent small sample drops within one measurement frame. Capacitance readings can be extracted from the colour map in Figure 3(a) by selecting the centre value for each drop. Figure 3(b) shows the resulting signal for a wide range of drop volumes. As expected, field focusing, the signal obtained for the smallest drops (1 μL) tends to have a larger magnitude (is more negative). However, the smaller drop width is on the same order of magnitude as the capacitor spacing and so the signal is measured across only one single electrode intersection. This means the signal for small drops is more prone to poor repeatability due to any slight displacement on the capacitor away from a targeted intersection. For drop volumes below 50 μL , the signal deviates substantially between drops of the same sample. Above 100 μL , the standard error between measured drops of the same electrolyte becomes less than 1.5% and the signal level stabilises. Figure 3b shows the range of sample volumes explored and the trade-off between small and large droplet deposition. There are no significant benefits from increasing droplet volume above 200 μL .

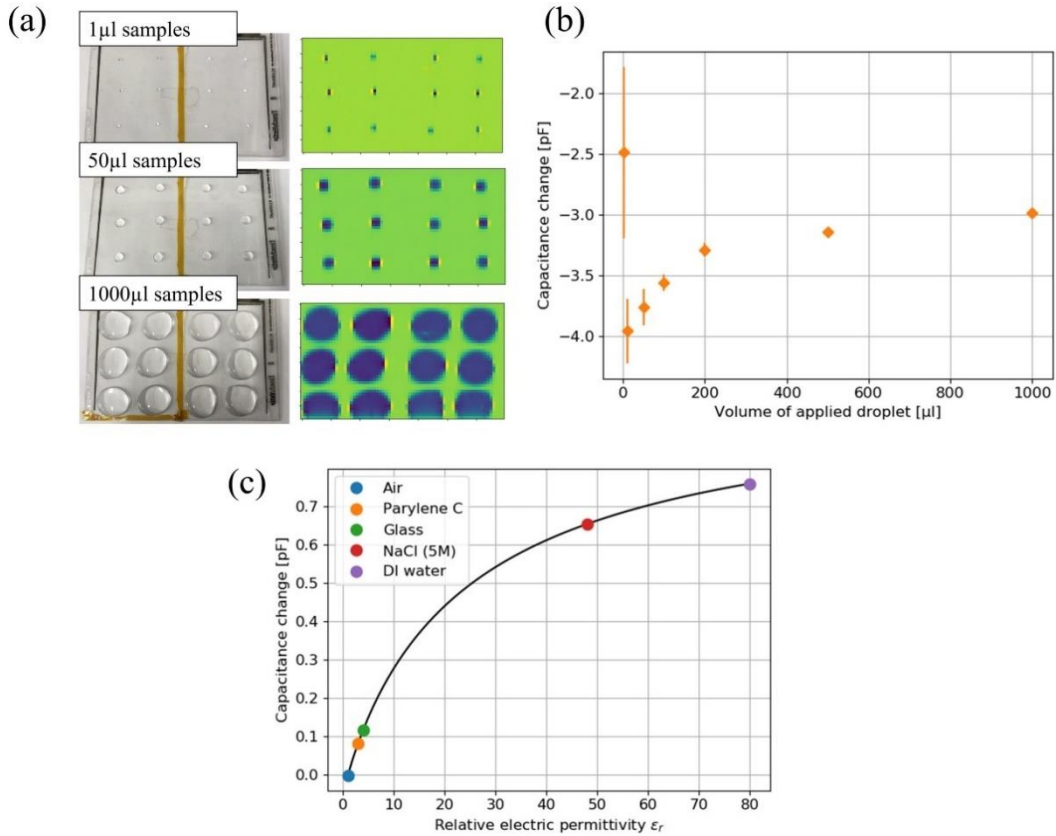


Figure 3: (a) Side-by-side view of a photograph of deposited drop volumes of 1 μL , 50 μL , and 1000 μL DI water (left) and the resulting capacitive signal on the sensor panel (right). Blue areas correspond to high field interaction, green areas signal no change to the dry sensor setting. (b) The capacitance signal (and deviation) spikes for 25 μL and stabilises beyond 200 μL of applied sample volume, as measured at the centre intersection of each detected drop ($n = 6$ drops per data point). (c) Relative permittivity-based simulation of increase in capacitance change compared to the dry screen for different material with relative permittivity from air, over 5M NaCl water, to de-ionised water [18]. This model does not take ion migration into account. The -40% difference in permittivity between 0M and 5M (=saturated) salt solution only causes a 13% drop in capacitance.

The simulation described in Section 2 allows us to explore the effect of the fluid drop's location on the screen and its content on the capacitance signal. Figure 3(c) uses the simulation to show the capacitance change when choosing different sample drop materials with a range of relative permittivity values. Water is a highly polar fluid and contributes significantly to the overall capacitance change at 0.8 pF. Selecting air as the drop material equals the simulation of a dry screen with 0 capacitance change. Experimentally, a 200 μL water drop evokes a capacitance change of (negative) 3-4 pF (depending on the purity of the DI water). The factor of around 4 between experimental and simulation magnitudes is attributed to the gain factor (amplification) set for the touchscreen controller. The simulation of a near-saturated salt solution (5 M NaCl) shows that the lower permittivity with the addition of salt will induce a smaller capacitance response, and so we will anticipate changes in capacitance of the order of 0.6 pF when moving to environmentally relevant samples.

To understand the importance of drop location, Figure 4a shows a 2d simulation of a droplet cross-section and visualises the displacement field resulting from a sample drop, depending on its lateral placement with respect to an activated electrode intersection. When the active capacitor is directly under the sample drop ($x = 0$), the polarisation within the water-based sample reaches a maximum, and hence gives a large change in the capacitance of the whole system when compared to a dry screen. For an electrode two positions from the centre of the drop ($x = 2$), the active intersection is within the drop boundary, and the polarisation remains strong. For measurements where the active electrodes are outside of the drop boundary, the polarisation drops at a near exponential rate. Additional details of the lateral sensitivity are provided in Supplementary Information S5. Figure 4(b) shows the results from a range of 3d simulations, where we see a predicted decrease in capacitance signal when the measured electrode intersection is further from the sample drop centre. Here, values on the y-axis are expressed in relation to signal magnitude for an intersection measured directly under the sample drop centre. The experimental data included in Figure 4(b) is in good agreement with the simulation. The vertical dashed line indicates the edge of the sample drop and a rapid decrease in signal is noted both experimentally and by simulation to the right of this line.

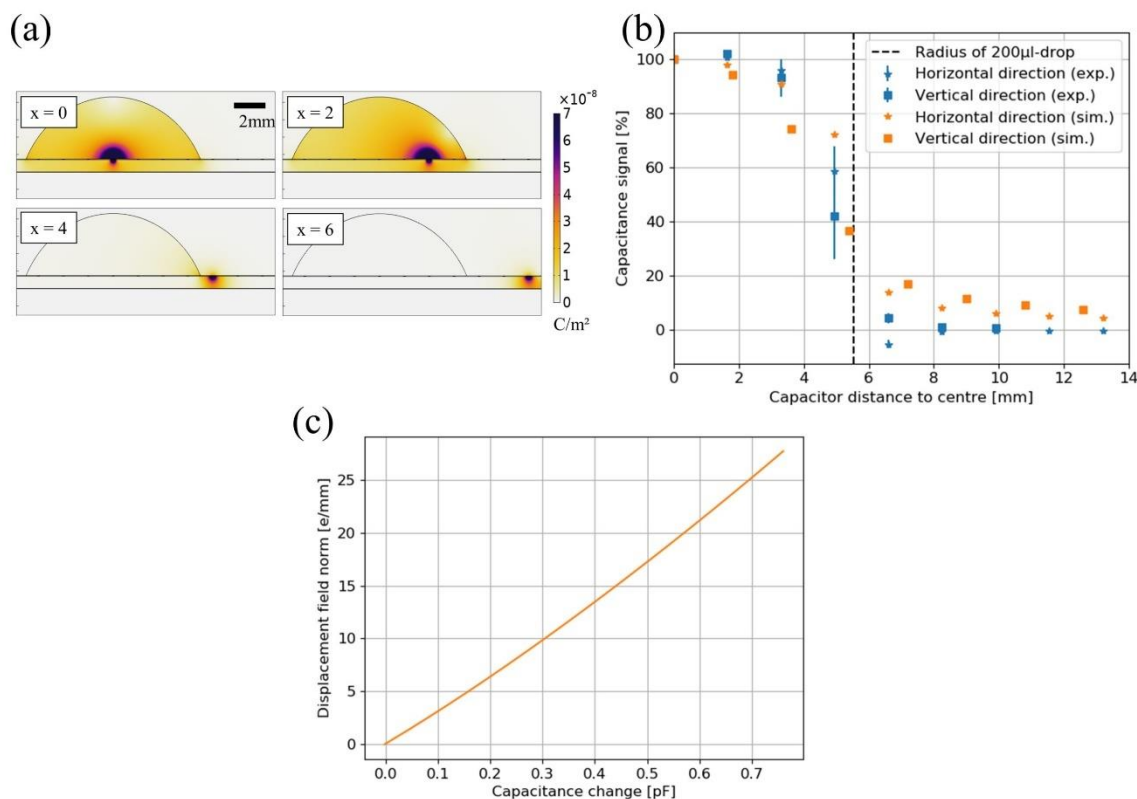


Figure 4: (a) The COMSOL simulation allows for showing the polarisation density P which would otherwise not be visible in an experiment. This illustration shows a 2d cross-section of a fixed sample drop with different top electrodes being activated, starting with an electrode in the centre of the sensor ($x = 0$). (b) The absolute mutual capacitance signal shown for electrode intersections measured in horizontal (stars) and vertical (squares) distances from a 200 μL drop centred at position 0. Measurements are plotted for both experiment (blue, $n = 6$) and simulation (orange, simulated in 3d-model). While the spatial resolution of both the actual and the simulated device is comparable, the signal cuts off more sharply beyond the droplet boundaries in the experimental device. (c) P correlates with the absolute mutual capacitance sensor signal as per Equation 2. The data shown in this plot was captured through the COMSOL simulation and confirms this correlation.

There is a 90% drop in signal for a 4 mm distance across the sample edge in the experiment, for both horizontal and vertical electrodes, while the simulation signal drops 80% horizontally and 50% vertically. While the signal in the simulation asymptotically approaches 0%, the experimental signal vanishes completely beyond the drop radius as it falls below the threshold of the noise filter in the software. The reading below the baseline observed for the horizontal distances shortly beyond the drop radius is an artifact from software overcompensation of the noise suppression. Figure 4c examines the correlation between displacement field, D , and capacitance change, C , as laid out in Equation (3) and (4), and shows a near-linear relationship between the two.

Guided by the observed characteristics of the touchscreen device in this section it is concluded that a sample volume of 200 μL per drop is suitable for further measurements. It is ideal to record the centre value of each detected drop to minimise drop edge effects and averaging over several samples (here $n = 6$) is preferable for consistency. Finally, this initial work shows that the displacement field, D , can be used as a proxy to qualitatively illustrate contributors to overall capacitance governed by permittivity. With this confidence in the approach to measuring the drop's polarisation field through capacitance readout directly from a touchscreen, the next steps are to better understand the role of any intermediate layer, essential for everyday use, and then test the approach with an example application, namely electrolyte sensing as a first example.

3.2. Role of an insulating layer

Environmentally sourced fluids, which will be the target samples for this sensor, contain ions and transport electric charges. As projected capacitive touchscreens measure capacitance rather than conductivity it is beneficial to separate conductive effects from capacitive effects by introducing an insulation layer. While this may be a manually deposited film in future applications, Parylene C was chosen for this purpose as it can be deposited in a highly controlled manner to allow detailed assessment. Figure 5(a) compares experimental measurements of a range of sodium chloride electrolyte concentrations firstly on an unprepared touchscreen

sensor (blue) and secondly on a screen with a 2 μm parylene C coating (orange). The polymer coated sensor can distinguish clearly between DI water and electrolyte, while the uncoated sensor does not. The latter also shows a higher level of noise across all tested samples.

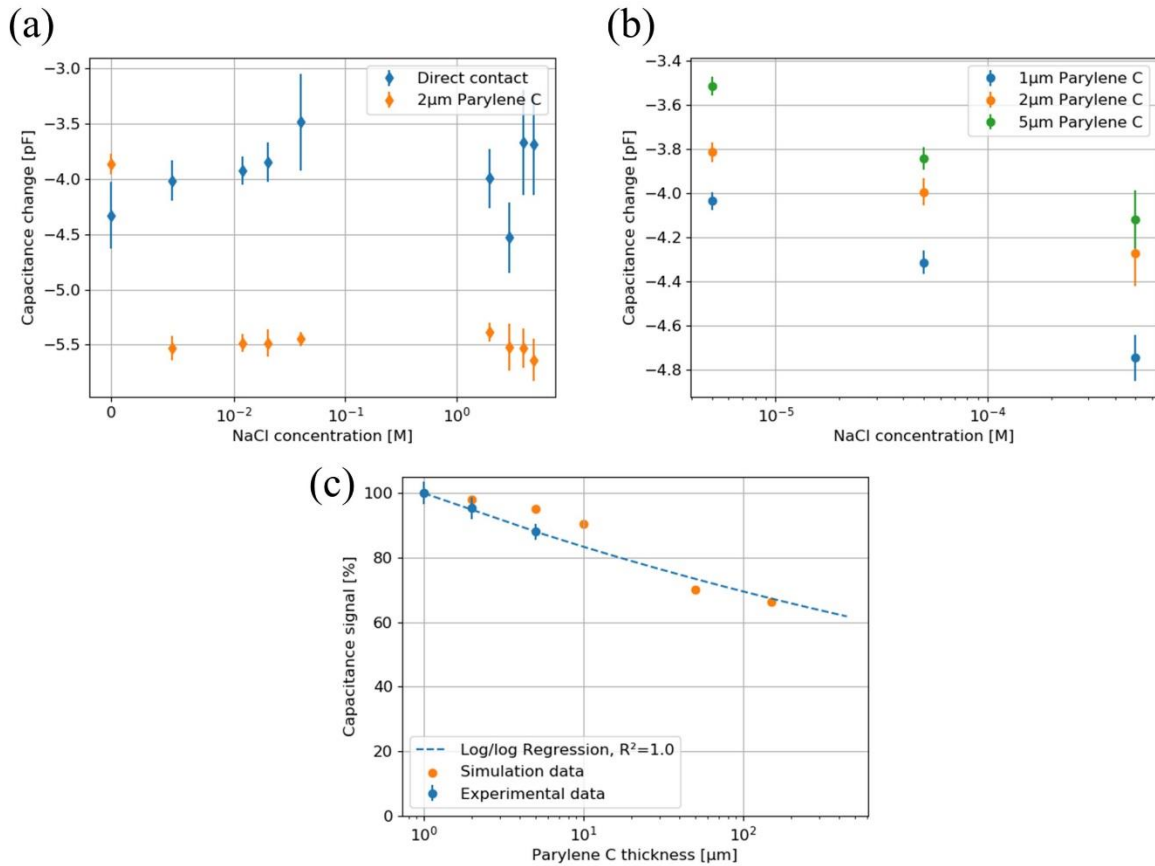


Figure 5: (a) The capacitance signal for sodium chloride solutions on a sensor without (blue) and with (orange) an insulating layer of parylene C. The layer increases the capacitive response of the system across the whole concentration range. A difference between DI water (0 M) and NaCl solution becomes significant. (b) Experimental signal versus sodium chloride concentration for three different parylene C fabrication thicknesses. The dynamic range tends to be larger for thinner parylene C. (c) The capacitance signal of DI water samples on thicker parylene C as predicted by simulation (orange) and experimentally, with a fit to the experimental data assuming a slow exponential decrease (blue).

An insulating layer is necessary for observing a response by the touchscreen to electrolyte concentration, and Figure 5(b) indicates that the absolute signal magnitude depends on both the parylene thickness and the concentrations of sodium chloride in the measured 200 μL drops. With decreasing parylene C thickness, the absolute range between capacitance values increases, however, for very thin 1 μm parylene C, the signal range resides close to the previously observed saturation threshold of -5.5pF. In Figure 5(c) a DI water drop is measured on an increasing parylene C layer separating it from the electrode intersection. The capacitance signal (relative to signal for a drop on 1 μm parylene C) decreases as the drop is moved further up within the fringe field. Results from a COMSOL simulation are included in Figure 5(c) and show the same behaviour over the experimental range. From the simulation it is possible to predict that this trend will continue for thicker layers beyond what was attempted experimentally. The experimental data is fitted with a log-log regression on the three measured data points showing a match with the general trend from simulated data. Typical smartphone touchscreen electrodes have a glass sheet cover. Although this thickness has been decreased to 450 μm by the industry in recent years, it will likely still cause a loss in signal strength and sensitivity compared to the thin layer parylene C used here [20]. At 450 μm parylene C thickness the experimental regression suggests 62% of the initial signal at 1 μm polymer thickness will remain. For the current work, a thickness of 2 μm is maintained based on these findings to ensure electrode insulation is maintained without compromising the capacitive coupling with the droplets.

3.3. Example application: measuring electrolyte concentration

The initial studies reported above show the capability to systematically measure aqueous drops with a capacitive coupling on the touchscreen sensor and that dissolved electrolytes can be detected. Here, we examine the sensitivity of this approach by targeting more environmentally challenging concentrations. Six different electrolytes are tested independently, and all samples are measured with a conductivity meter for reference. As demonstrated earlier, electric field focusing is influenced by the relative permittivity ϵ_r of a fluid sample. High content of salt in water indeed affects ϵ_r , e.g., the permittivity of water halves as it is saturated with sodium chloride at a concentration beyond 6 M [21]. For electrolyte concentrations on the order of 10^{-3} M, such as typical in biological fluids, the effect on its relative permittivity is small and we would expect only little (less negative) capacitance change. The results, however, show an increased (more negative) capacitance change. There appears to be high sensitivity potentially able to resolve sub-ppm levels of contamination, such as those relevant to trace metal detection in contaminated water and soil. Figure 6(a) shows the recorded conductivity for all samples before deposition on the touchscreen device. For reference, sodium acetate has been included in the measurement, which is also classified as mono-valent, similar to sodium chloride, but has an anion which is poorly dissociated. On the log-log-scale, we observe a linear correlation with the anion concentration. The fit lines overlap for all chloride-based electrolytes but iron, which can be attributed to its redox properties. Sodium acetate has a different anion and its conductivity resides below the chloride-based electrolytes. The slope is ≈ 1 for all electrolyte types, consistent with the linear relationship also on a non-logarithmic scale. Details on the regression results can be found in the Supplementary Information, Table A2.

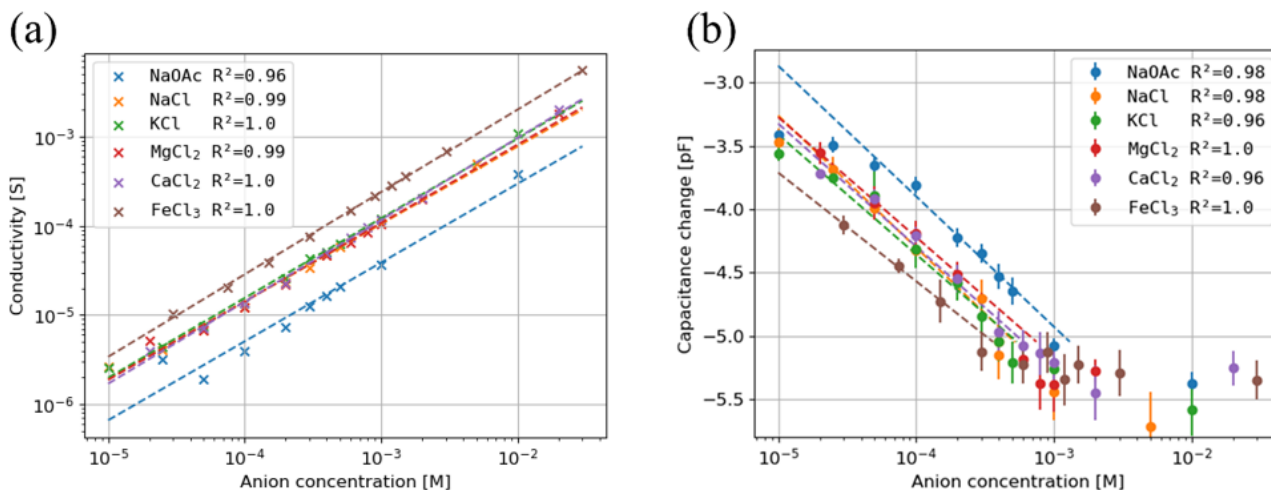


Figure 6: (a) The measured conductivity for different electrolytes with concentrations in the μM regime using a conductivity instrument. The dotted lines show linear regressions with the corresponding R-squared-value (between 0 for no, and 1 for perfect accordance of data with fit, see Table A3, S.I.). (b) The same electrolytes measured for capacitance on the touchscreen set-up. A capacitance threshold of -5.05 pF before the sensor reaches saturation was set for the linear regression to take values into account, see Table A3, S.I.

The same solutions are measured on the touchscreen sensor using the best-practice defined so far in this paper, and plotted in Figure 6(b). The absolute capacitance magnitude increases linearly with increasing ion concentration on a semi-log scale for all tested electrolytes. The linearity breaks down for ion concentrations above 500 μM , when the sensor begins to reach saturation. This saturation was observed earlier in Section 3.2. Here, we see the saturation concentration threshold differs slightly depending on the electrolyte type. However, it is consistently reached for capacitance values below -5.05 pF. Moreover, sodium and potassium chloride (mono-valent cation), magnesium and calcium chloride (bi-valent cation), and iron chloride (tri-valent cation) each have a similar slope (about 1 pF per decade change in concentration) but show an offset (see Supplementary Information S5); replotting the data against anion concentration adjusts for the charge of the cation.

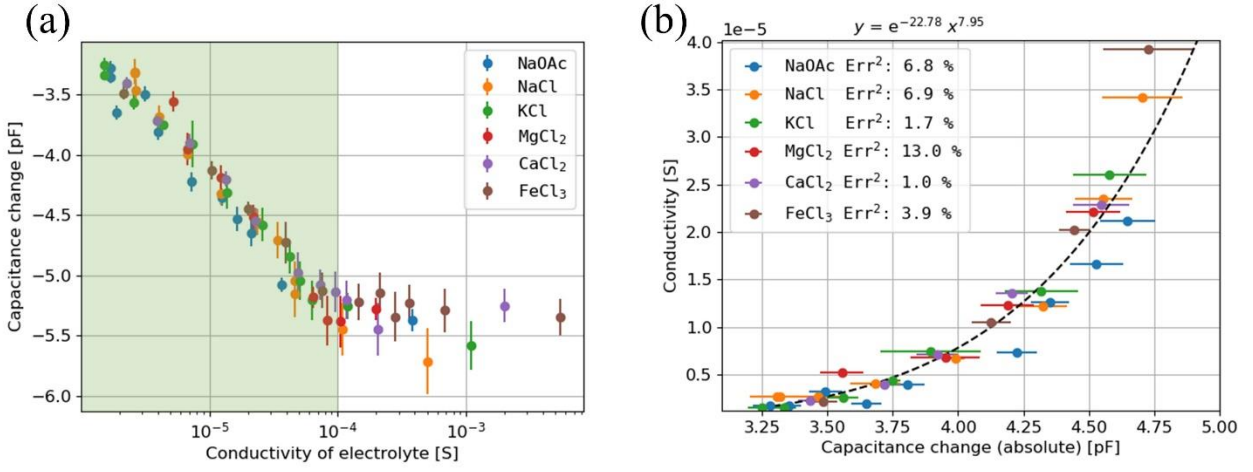


Figure 7: (a) The capacitive signal obtained with the touch sensor on y correlated with the conductivity for all electrolytes on the x -axis. The sensitive range is highlighted in green. (b) Calibration (dotted line, equation above) based on the linearity on a semi-log scale shown in (a) using the whole dataset combined. Each electrolyte's mean squared deviation from the calibration is indicated in the legend. While the touchscreen response to potassium chloride (green) and calcium chloride (purple) matches their actual conductivity within 2% deviation, magnesium chloride (red) shows a higher deviation of 13%.

Taking both the above data sets together allow for the correlation between electrolyte conductivity and touchscreen capacitance, as plotted in Figure 7(a). This shows a semi-logarithmic trend for all electrolytes below 100 μS before the sensor saturates, at which point the capacitance signal no longer changes with an increase in electrolyte conductivity. The conductivity behaves consistently with capacitance for both types of anion/cation. Finally, Figure 7(b) shows the calibration for conductivity with each corresponding capacitance based on a linear-fit in the semi-log representation for all data combined. We notice a tight fit particularly for potassium and calcium chloride with less than 2% deviation from the general calibration. Conclusively, we note the minimal presence (around μM concentration regime) of ions in DI water has a significant influence on capacitive readings. As discussed earlier the relative permittivity of the electrolyte is not altered notably by such low concentrations of salt, indicating that effects come into play that cannot be explained by a model solely based on permittivity. At this point, we anticipate effects of the electric double layer of ions assembling on the charged touchscreen surface contributing to the observed changes in capacitance. Equation 5 suggests the conductivity κ is attributed to the increased amount of charge transported per ion and counteracted by the increased mass (decreased mobility μ_i) of high-valency ions. It is found that for dilute solutions the conductivity can be expressed as the sum of all types of ions n_i multiplied with their charge $q_i = z_i e$ and their mobility μ_i , where e is the elementary charge and z is the ion valency [22].

$$\kappa = \sum n_i q_i \mu_i \quad (5)$$

Equation 6 is known as the Nernst-Planck equation for migration in a static electric field. Following this equation, negatively charged anions migrate within the electrolyte with a diffusion flux \mathbf{J}_i towards the positive electrode potential on the parylene C interface near the active touchscreen intersection. This migration constitutes of concentration gradient-driven diffusion with rate D_i , and migration due to the electric field of the applied potential U , where F is the Faraday constant.

$$\mathbf{J}_i = -D_i \nabla c_i - z_i \mu_i F c_i \nabla U \quad (6)$$

At the interface, their concentration c_i increases and they form a Debye double layer (DL). This DL has its own capacitance which adds to the capacitance signal we measure [23, 24]. In the low concentration regime, the effects ion transport due to the electric field dominate for conductivity and capacitance and the same signal

trend is observed in our experiments. The touchscreen sensor saturation at concentrations approaching the mM regime is, however, only observed for capacitance and not for conductivity experiments. Hence, we anticipate a connection to the charged capacitor (parylene C) surface where ions can assemble on the positively charged interface. The effect is seen for all ionic species and appears to be governed by the anion charge. For increasing concentrations, the surface charge compensation through the electrolyte grows. As ions further populate the double layer, they are limited by their spatial dimension determined by the electrostatic shell. This is expected to limit the number of charged ions that can assemble in the inner Helmholtz layer of the DL and leads to saturation above its capacitance threshold. More complex electrochemical simulation tools may be explored in future work to help shine a light on ion anion-cation interactions and interfacial effects for further understanding of the sensing mechanisms on a capacitive touchscreen.

4. Conclusion

In this work we propose and explore the use of a standard industry mutual capacitive touchscreen as a sensing tool for ion concentrations in an electrolyte, sensing directly from drops placed on the screen surface. A robust approach was identified through examination of suitable droplet volumes and a thin insulating layer to ensure the ITO electrodes were not exposed. This initial work provides exciting design guidance for future research, highlighting the trade-offs with decreasing drop size and highlighting the importance of the insulating layer between the electrodes and the sample. The drop volume, positioning and spacing layer conclusions were examined from the context of COMSOL simulations to help explain the influences on the capacitive coupling. An initial application of measuring electrolyte concentration was demonstrated and the rate of capacitance change per anion concentration unit is consistent across all tested electrolytes. The tested projected capacitive touchscreen sensor showed a tight semi-log correlation with the conductivity of electrolytes below 100 μ S. This correlation is dependent on anion concentration and nearly independent of the tested cation (mono, bi, or tri-valent metal cation), although the redox ferrous cation did not overlay fully with the other cations and the weakly ionic acetate anion showed a reduced range. While this detection window lies below typical concentrations of ions in biological fluids, it matches that of trace metal contaminants in drinking water and the presence of soil nutrients such as phosphate, nitrate, phosphate and potassium [25, 26]. The work demonstrated that the measurement does not require direct contact between the sample and the electrodes for conductivity measurements. This prevents degradation, enhances the ease of cleaning, and shows the potential to be translated in the future towards use with existing mobile technologies. Each sample drop in this study covers more than 25 electrode intersections, each of which acts as an individual sensor pixel. This lends itself to multiplexing applications, so we anticipate capacitive touchscreen sensing will be beneficial beyond the scope of electrolyte measurements. Future work will tackle translating to a broader range of bio- and environmental sensing scenarios with selective analyte detection and an implementation of our concept on a mobile device outside the laboratory environment.

Supporting Information

Additional supporting figures and tables are provided in Supplementary Information.

Acknowledgement

This research was supported by the UK Engineering and Physical Sciences Research Council (EPSRC) grant EP/L015889/1 for the EPSRC Centre for Doctoral Training in Sensor Technologies and Applications. We also thank MSolv Ltd. for supplying touchscreen device samples and in particular Phil Rumsby and Adam Brunton for technical support and fruitful discussions. We thank TouchNetix for providing readout hardware for the capacitance measurements. We thank Dr. Ljiljana Fruk and Christoph Franck from the Department of Chemical Engineering and Biotechnology of University of Cambridge for providing us with electrolyte testing solutions.

References

- [1] Steinhubl, S. R., Muse, E. D., & Topol, E. J. (2015). The emerging field of mobile health. In *Science Translational Medicine* (Vol. 7, Issue 283, p. 283rv3). American Association for the Advancement of Science. <https://doi.org/10.1126/scitranslmed.aaa3487>
- [2] Zhang, D., & Liu, Q. (2016). Biosensors and bioelectronics on smartphone for portable biochemical detection. *Biosensors and Bioelectronics*, 75, 273–284. <https://doi.org/10.1016/j.bios.2015.08.037>.

- [3] Majumder, S., & Deen, M. J. (2019). Smartphone sensors for health monitoring and diagnosis. In *Sensors (Switzerland)* (Vol. 19, Issue 9). MDPI AG. <https://doi.org/10.3390/s19092164>.
- [4] More, A. (2020). Capacitive Touch Screen Market Growth 2020 Global Industry Size, Analysis, Share, Trends, Market Demand, Growth, Opportunities and Forecast 2025 - MarketWatch. Marketwatch.Com.
- [5] Phares, R., & Fihn, M. (2012). Introduction to Touchscreen Technologies. In *Handbook of Visual Display Technology* (pp. 935–974). Springer Berlin Heidelberg. https://doi.org/10.1007/978-3-540-79567-4_63.
- [6] Walker, G. (2012). A review of technologies for sensing contact location on the surface of a display. *Journal of the Society for Information Display*, 20(8), 413–440. <https://doi.org/10.1002/jsid.100>.
- [7] Kolokowsky, S., & Davis, T. (2009). Touchscreens 101: Understanding Touchscreen Technology and Design. Cypress, June 2009, 1–5. <http://www.cypress.com/file/95156/download>.
- [8] Won, B. Y., & Park, H. G. (2012). A touchscreen as a biomolecule detection platform. *Angewandte Chemie - International Edition*, 51(3), 748–751. <https://doi.org/10.1002/anie.201105986>.
- [9] Won, B. Y., Ahn, J. K., & Park, H. G. (2016). New Surface Capacitive Touchscreen Technology to Detect DNA. *ACS Sensors*, 1(5), 560–565. <https://doi.org/10.1021/acssensors.6b00040>.
- [10] Lee, J. Y., Won, B. Y., & Park, H. G. (2018). Label-Free Multiplex DNA Detection Utilizing Projected Capacitive Touchscreen. *Biotechnology Journal*, 13(2), 1700362. <https://doi.org/10.1002/biot.201700362>.
- [11] Cassivi, A., Dorea, C. C., Johnston, R., & Waygood, E. O. D. (2018). Access to drinking water: Time matters. *Journal of Water and Health*, 16(4), 661–666. <https://doi.org/10.2166/wh.2018.009>.
- [12] de Villiers, C. A., Lapsley, M. C., & Hall, E. A. H. (2015). A step towards mobile arsenic measurement for surface waters. *The Analyst*, 140(8), 2644–2655. <https://doi.org/10.1039/C4AN02368D>.
- [13] Sinfield, J. V., Fagerman, D., & Colic, O. (2010). Evaluation of sensing technologies for on-the-go detection of macro-nutrients in cultivated soils. *Computers and Electronics in Agriculture*, 70(1), 1–18. <https://doi.org/10.1016/j.compag.2009.09.017>.
- [14] Crespo, G. A. (2017). Recent Advances in Ion-selective membrane electrodes for in situ environmental water analysis. *Electrochimica Acta*, 245, 1023–1034. <https://doi.org/10.1016/j.electacta.2017.05.159>.
- [15] Kruse, P. (2018). Review on water quality sensors. *Journal of Physics D: Applied Physics*, 51(20). <https://doi.org/10.1088/1361-6463/aabb93>.
- [16] Mayer, S., Xu, X. and Harrison, C. 2021. Super-Resolution Capacitive Touchscreens. In *Proceedings of the 39th Annual SIGCHI Conference on Human Factors in Computing Systems (May 8 - 13, 2021)*. CHI '21. ACM, New York, NY. Article 12, 1–10. <https://doi.org/10.1145/3411764.3445703>.
- [17] Ortigoza-Diaz, J., Scholten, K., Larson, C., Cobo, A., Hudson, T., Yoo, J., Baldwin, A., Hirschberg, A. W., & Meng, E. (2018). Techniques and considerations in the microfabrication of parylene c microelectromechanical systems. *Micromachines*, 9(9). <https://doi.org/10.3390/mi9090422>.
- [18] Olofsson, J., Levin, M., Strömberg, A., Weber, S. G., Ryttsén, F., & Orwar, O. (2005). Generation of focused electric field patterns at dielectric surfaces. *Analytical Chemistry*, 77(14), 4667–4672. <https://doi.org/10.1021/ac0502302>.
- [19] Persson, R. A. X. (2017). On the dielectric decrement of electrolyte solutions: A dressed-ion theory analysis. *Physical Chemistry Chemical Physics*, 19(3), 1982–1987. <https://doi.org/10.1039/c6cp07515k>.
- [20] Corning Inc. (2020). Corning Gorilla ® Glass Victus TM. Globe Newswire. <https://www.globenewswire.com/news-release/2020/07/23/2066674/0/en/Corning-Introduces-Corning-Gorilla-Glass-Victus-The-Toughest-Gorilla-Glass-Yet-For-Mobile-Consumer-Electronics.html>.
- [21] Hasted, J. B., Ritson, D. M., & Collie, C. H. (1948). Dielectric properties of aqueous ionic solutions. Parts I and II. *The Journal of Chemical Physics*, 16(1), 1–21. <https://doi.org/10.1063/1.1746645>.
- [22] Zhang, W., Chen, X., Wang, Y., Wu, L., & Hu, Y. (2020). Experimental and modeling of conductivity for electrolyte solution systems. *ACS Omega*, 5(35), 22465–22474. <https://doi.org/10.1021/acsomega.0c03013>.
- [23] Khademi, M., & Barz, D. P. J. (2020). Structure of the Electrical Double Layer Revisited: Electrode Capacitance in Aqueous Solutions. *Langmuir : The ACS Journal of Surfaces and Colloids*, 36(16), 4250–4260. <https://doi.org/10.1021/acs.langmuir.0c00024>.
- [24] Opekar, F., Tůma, P., & Štulík, K. (2013). Contactless impedance sensors and their application to flow measurements. In *Sensors (Switzerland)* (Vol. 13, Issue 3, pp. 2786–2801). <https://doi.org/10.3390/s130302786>.
- [25] Arienzo, M., Christen, E. W., Quayle, W., & Kumar, A. (2009). A review of the fate of potassium in the soil-plant system after land application of wastewaters. *Journal of Hazardous Materials*, 164(2–3), 415–422. <https://doi.org/10.1016/j.jhazmat.2008.08.095>.
- [26] Gondwe, R. L., Kinoshita, R., Suminoe, T., Aiuchi, D., Palta, J. P., & Tani, M. (2020). Available Soil Nutrients and NPK Application Impacts on Yield, Quality, and Nutrient Composition of Potatoes Growing during the Main Season in Japan. *American Journal of Potato Research*, 97(3), 234–245. <https://doi.org/10.1007/s12230-020-09776-2>.

Supplementary Information

S1. Parylene C coating

Prior to the coating, all electrical contacts normally used for interfacing with the sensor were covered with heat resistant Kapton tape to retain their conductive surface. For a $1.0\ \mu\text{m}$ coating 0.4 g, and for $5.0\ \mu\text{m}$ 3.25 g dimer was filled into the machine. After the machine is filled and vents are turned off, the vacuum pump is enabled. As the pressure drops from 1000 mbar to 50 mbar the machine is filled with liquid nitrogen for cooling until a vacuum of around 7 mbar establishes. Then, the furnace and vaporize setting is enabled to start the deposition programme. As soon as the furnace reaches $690\ \text{C}$ (around 30 min) the coating starts automatically (around 1 h to complete). The sample can be removed after the vaporizer cooled down to about $40\ \text{C}$ and after the chamber is carefully vented. The parylene C layer thickness is then verified using a profilometry microscope.

S2. Probe stability

To check sensor stability, the same measurement routine was repeated six times over a period of 2 weeks with the same $500\ \mu\text{M}$ potassium chloride sample, and the results are plotted in Figure A1. The DI water for cleaning and reference was taken from varying reservoirs. The potassium chloride measurement maintains a stable capacitance reading with $\pm < 1\ \%$ error. The reference DI water measurements before and after each electrolyte test are consistent within each measurement day - at times the pre-electrolyte value is higher, at others the post-electrolyte measurement value for water turns out higher. It is notable that the sensor is very sensitive to small ionic contamination within the DI water as the readings vary over time. DI water is susceptible to ionic impurities in daily handling when exposed to air as it is prone to absorb carbon dioxide and produce carbonic acid.

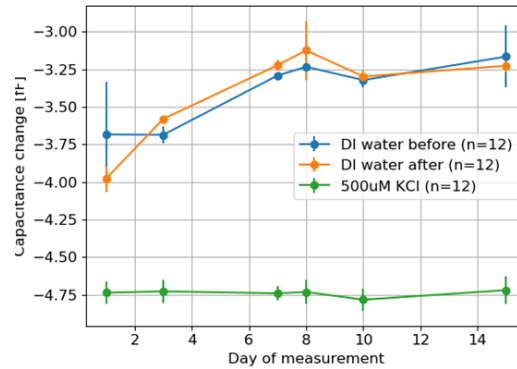


Figure A1: The same potassium chloride sample measured over a period of 2 weeks taking a reference measurement with DI water before and after. The touchscreen performs stably for the potassium chloride sample over time and returns to its default response after cleaning with DI water.

S3. Drop spread on touchscreen surface

For the computer model the geometry of a sample drop deposited on the parylene C coated touchscreen surface needed to be approximated. We use the section of a sphere to resemble the shape of a drop. The boundary parameters are extracted from experimental observations.

For a DI water drop of $V_0 = 200\ \mu\text{L}$ in volume, a footprint on the sensor of diameter $r_0 = 5.6\ \text{mm}$ was experimentally observed ($n = 24$ drops). As illustrated in Figure A2, the drop height is observed to be significantly flatter than a half sphere. Experimental measurement of the drop height proved difficult; however, it can be solved for by matching the deposited volume with the measured perimeter radius via a volume integral for a sphere section.

Generally, to calculate the volume V one can integrate across all the circle areas contained within a sphere from $-R$ to R :

$$V(R) = \pi \int_{-R}^R F^2 dz \quad (7)$$

In this specific case, we would like to solve for a section of the sphere only. The radius r_0 at the sphere section base is $5.6\ \text{mm}$ at height $z_0 > 0$. The target sphere of which our drop cap is a section of has an unknown radius of $R > z_0$ at its widest point at z_0 .

$$V(z_0, R) = \pi \int_{-z_0}^R z_0(z, R)^2 dz \quad (8)$$

where $r_0 = \sqrt{R^2 - z_0^2}$.

This equation can be solved which gives a base radius R of 6.17 mm for the sphere section to match the 200 μL volume with section radius r_0 . The estimated value was used for all simulations in this article.

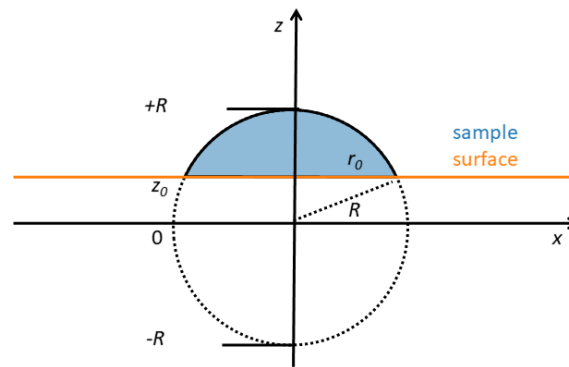


Figure A2: Cross section 2D-drawing of the sample on the touchscreen surface shaped as a sphere cap. The integral for its volume can be solved analytically to get the sphere section necessary for the simulation geometry.

S4. Sub grid structure between top electrodes

Upon close inspection under the interferometer, it becomes visible that the manufacturer of the touchscreen panel has not removed the ITO in between active electrodes but diced it up into an electrically insulated, passive sub-grid structure of around 200 μm width per rectangle, compare Figure A3. An initial computer simulation indicated this grid consistently decreases the signal magnitude by about 10 % without significant implications on sensitivity. As high aspect ratio models increase the mesh complexity, and hence, computation time, in this sub-grid was not further considered in the model. However, the model still contains very small elements such as the thin parylene C layer (few μm) and macroscopic details such as the sample drop or the electrode spacing (mm range).

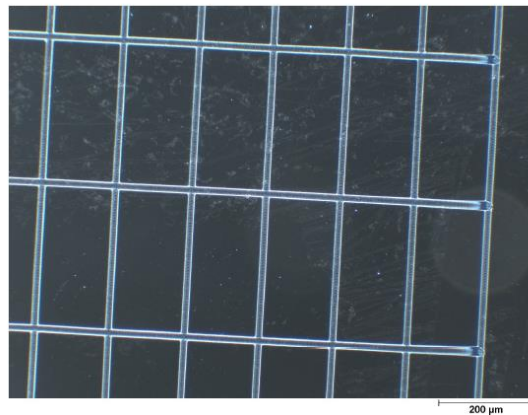


Figure A3: Interferometer image of the top ITO structure of the touchscreen with an electrically insulated structure and a continuous electrode on the right. The left area is in between top electrodes and diced-up via laser-ablation by the manufacturer.

S5. COMSOL finite element meshing

The mesh has been optimised for a suitable compromise between element quality and time/memory restrictions of the computing machine. Figure A4(a) shows a histogram of the mesh elements generated by the simulation software while Figure A4(b) visualises the 150,000 finite mesh elements this 3D structure was divided into. The mesh is user-adjusted to the touchscreen model by setting the maximum element size to the drop footprint radius ($R = 5.6$ mm) and the minimum element size to the smallest feature (for this simulation: parylene C height 20 μm). The maximum element growth rate is set to 2, curvature factor to 1 and the resolution of narrow regions to 0.1. Mesh smoothing iterations are set to 4 and the optimisation level is adjusted to high (large, small, and inverted curved elements to be avoided by the software).

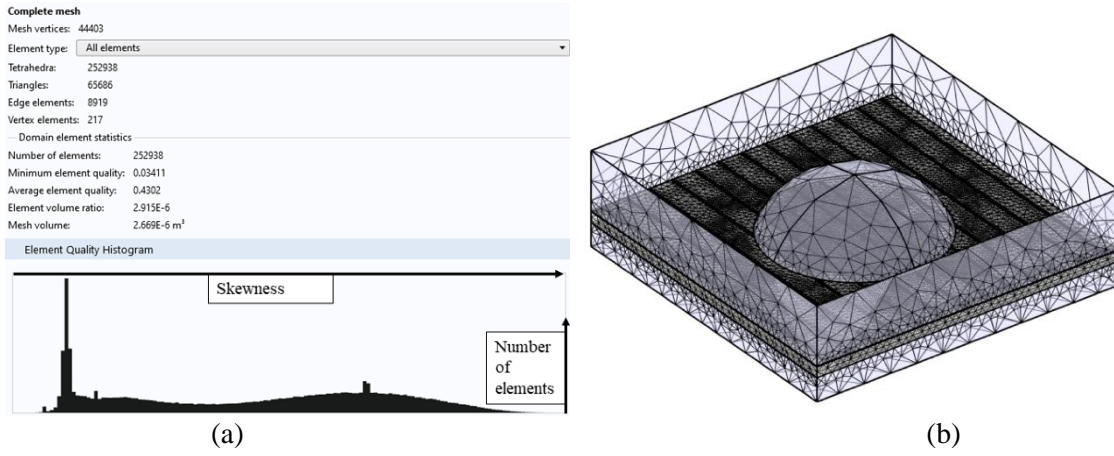


Figure A4: (a) Free tetrahedral finite element meshing of the 3D model used for simulation. (b) The element properties and quality of mesh elements.

S6. COMSOL displacement field and capacity link

The electric displacement field D is used in this work to visualise the local contribution of the electric fringe field to the overall capacitance C outputted by the simulation software. Equation 3 and equation 4 indicate a correlation between $\int_V^0 D$ and C . To validate this through our simulation Figure A5(a) and A5(b) contrast the displacement field integrated across all volume elements within the same 3D-model with the resulting Maxwell capacitance reading used as a measure for signal in the simulation throughout this article.

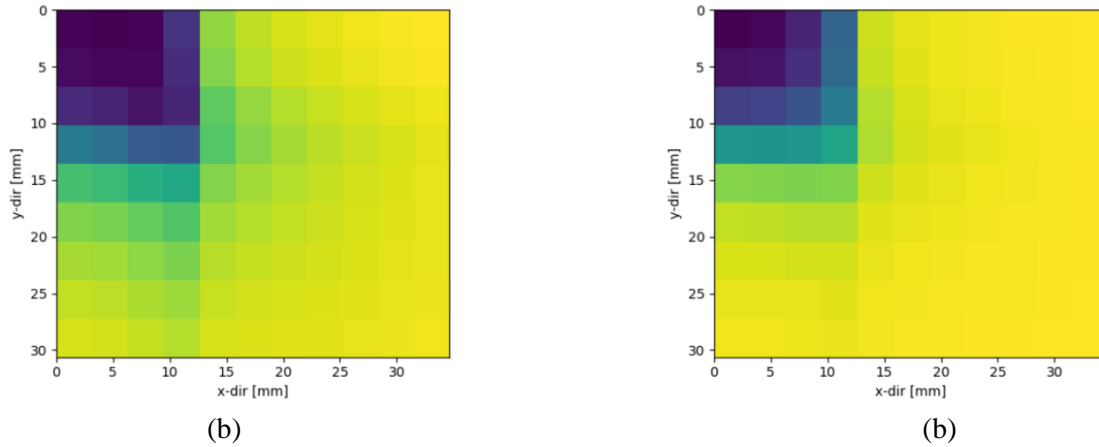


Figure A5: (a) The electric displacement field $\int_V^0 D$ integrated across all local volume elements for each measured electrode intersection. (b) The global Maxwell capacitance C for each intersection. Each pixel corresponds to one simulation per active electrode pair. The plot origin is in the centre of a 200 μ L water drop. The colour coding goes from low (yellow) to high (blue) relative to the range of recorded values. The correlation laid out in the theory of Eq. 2 – Eq. 4 reflects in the simulations.

S5. COMSOL displacement field and capacity link

The slope for all types of electrolytes in the detection window measured on the capacitive touchscreen sensor was nearly identical, but an offset is observed depending on the cation charge (electrolyte valency), see Figure A6. Due to the positive top electrode of the capacitive touchscreen sensor the capacitance change is dominated by the negative ions in solution, hence this offset can be corrected for by scaling the x-axis with a factor of 2 for magnesium and calcium chloride and 3 for iron chloride.

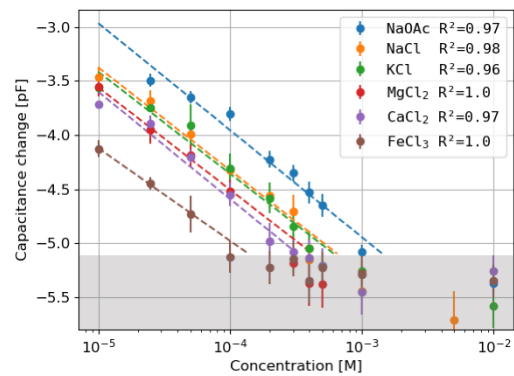


Figure A6: (a) The touchscreen capacitance changes for different electrolytes depending on total ion concentration (not adjusted to anion concentration).

Table A1: Simulation input parameters.

Name	Expression	Description
h_glass	0.7[mm]	Height of the TS glass
h_ito	w_laser	Thickness of ITO electrode
w_glass	n_xelectrodes*top_pitch	Width of TS glass
w_line	158[um]	Width of top electrode
h_parylene	20[um]	Default height of parylene
h_air	R	Height of the air filled space above TS surface
drop_xpos	w_glass/2	Default drop x-position (glass centre)
drop_ypos	w_glass/2	Default drop y-position (glass centre)
w_laser	30[um]	Width of the insulating line between electrodes
top_pitch	1.6[mm]	Spacing of x-electrodes (horizontal)
bottom_pitch	1.85[mm]	Spacing of y-electrodes (vertical)
n_xelectrodes	17	Number of x-electrodes
n_yelectrodes	floor(w_glass/bottom_pitch)-1	Number of y-electrodes
x_active	8	Default active x-electrode (glass centre)
y_active	6	Default active y-electrode (glass centre)
r0	5.6[mm]	Measured sphere section radius of sample
R	6.17[mm]	Underlying sphere radius of sample
z0	sqrt(R2-r02)	Height underlying sphere
Er	80	Relative permittivity of sample
Er_air	1	Relative permittivity of air
Er_ito	4	Relative permittivity of ITO
Er_glass	4.2	Relative permittivity of glass
Er_parylene	2.65	Relative permittivity of parylene C
v0	1[V]	Terminal voltage of top electrode to ground

Table A2: Conductivity versus concentration: Log/log linear regression intercept, slope, and fit correlation of the regression lines for Figure 6a.

Electrolyte	Intercept [log ₁₀ S]	Slope [log ₁₀ S/log ₁₀ M]	R ²
NaOAc	-1.76	0.88	0.96
NaCl	-1.38	0.87	0.99
KCl	-1.24	0.89	1.0
MgCl ₂	-1.07	0.88	0.99
CaCl ₂	-0.91	0.92	1.0
FeCl ₃	-0.41	0.92	1.0

Table A3: Capacitance versus concentration: Log/log linear regression intercept, slope, and fit correlation of the regression lines for Figure 6b.

Electrolyte	Intercept [pF]	Slope [pF/log ₁₀ M]	R ²
NaOAc	-8.32	-1.11	0.98
NaCl	-8.47	-1.04	0.98
KCl	-8.12	-0.94	0.96
MgCl ₂	-8.29	-0.95	1.0
CaCl ₂	-8.54	-0.99	0.98
FeCl ₃	-8.4	-0.86	1.0